

Article

Hierarchical Core/Shell Structured Ag@Ni(OH)₂ Nanospheres as Binder-Free Electrodes for High Performance Supercapacitors

Sa Lv ^{*}, Xuefeng Chu, Fan Yang, Huan Wang , Jia Yang, Yaodan Chi and Xiaotian Yang ^{*}

Jilin Provincial Key Laboratory of Architectural Electricity & Comprehensive Energy Saving, School of Electrical Engineering and Computer, Jilin Jianzhu University, Changchun 130118, China; stone2009@126.com (X.C.); ctpnxxn@163.com (F.Y.); whuan@ciac.ac.cn (H.W.); yangjia@jlju.edu.cn (J.Y.); chiyaodan@jlju.edu.cn (Y.C.)

^{*} Correspondence: lvsa82@163.com (S.L.); hanyxt@163.com (X.Y.); Tel.: +86-0431-8456-6181 (S.L.)

Received: 27 January 2019; Accepted: 21 February 2019; Published: 24 February 2019



Abstract: Hierarchical Ag@Ni(OH)₂ nanospheres were achieved directly on copper foam substrate through a convenient two-step process. Ag nanoflowers were formed on copper substrate by galvanic replacement technology between AgNO₃ and copper foam followed by electrodeposition of a layer of Ni(OH)₂. Ag nanostructures as cores not only dominated the final morphology of the composites, but also improved the electrical conductivity, increased the specific surface area of the active electrode material, and even directly participated in the electrochemical reactions. The resulted Ag@Ni(OH)₂ nanospheres could be directly used as high-performance binder-free electrodes and exhibited enhanced electrochemical performance with a high specific capacitance of 1.864 F cm⁻² and long cycling lifespans of 90.43% capacity retaining after 3000 cycles.

Keywords: electrodeposition; Ag@Ni(OH)₂ nanospheres; electrode material; supercapacitor

1. Introduction

Supercapacitors, as one of the most efficient energy storage and conversion devices have attracted ever-increasing interest due to their fast charging–discharging rate, remarkable power density and long cycling lifespans [1]. It is generally believed that the electrochemical performances of supercapacitor depend mainly on the electrode materials [2]. Among these candidates, pseudocapacitive materials of transition metal hydroxides/oxides, including Ni(OH)₂/NiO [3], Co₃O₄ [4] and MnO₂ [5] have attracted considerable attention because of their reversible redox behavior, reasonable cost and environmentally friendly characteristics [6,7]. Ni(OH)₂ is considered as the most competitive candidate owing to its high chemical stability, natural abundance of nickel compounds and high theoretical specific capacity. A large number of in-depth explorations have been performed on optimizing the performance of Ni(OH)₂. But the relatively low conductivity and active surface areas often limit the effective utilization of electrode materials, and lead to the reduction of energy and power density. To address these problems, three strategies have been conceived: (1) Constructing hybrid materials by adding components or elements with high conductivity, such as graphene, Ag, Au and Cu; (2) Designing various hierarchical structures, forming porous structure or reducing particle size in order to increase the specific surface area of the active materials; (3) Adopting chemically stable conductive substrates with proper surface modification, such as copper foam [8], stainless steel mesh [9], cotton textile [10] and paper [11]. For example, Gong and coworkers [12] fabricated Ni(OH)₂-Cu hybrid electrode by hydrothermal method, which exhibited an ultrahigh areal capacitance of 8.66 F cm⁻² at 1 mA cm⁻². The prominent enhancement is attributed to the highly conductive path provided by the metallic Cu layer, which facilitates charge transport and benefits fast redox

reaction. Jeyasubramanian et al. [13] reported the growth of MnO_2 nanostructures on hierarchical Cu nanoleaves via a two-step electrodeposition, which demonstrated a high specific capacitance of 486 F g^{-1} at 1 mA cm^{-2} . Shin and coworkers [14] described the decoration of Co_3O_4 by Ag nanoparticles using chemical immersion method, and the composite electrode achieved a superior specific capacitance of 958 F g^{-1} . These works revealed that the reasonable design and construction of metal hydroxides/oxides-based materials with conductive reinforcement is an effective method to enhance the electrochemical performances of the hybrid electrodes.

Previous published papers have confirmed the use of Ag as an enhancement component owing to its stability, high electrical conductivity and electrochemical activity. Therefore, it is reasonable to believe that Ag/ $\text{Ni}(\text{OH})_2$ composite electrode will have excellent electrochemical properties. The existing technologies to achieve Ag/ $\text{Ni}(\text{OH})_2$ composite usually involve two steps. The initial Ag nanostructures could be obtained by various methods, such as electrodeposition and hydrothermal method [15]. After that, the metal hydroxides/oxides were grown on the Ag electrode surface via hydrothermal or electrodeposition [16,17]. The hierarchical structure is helpful to exert the synergistic effect between each component and enhances the overall electrochemical properties thereby. However, the resulting samples in a powdered state must be pressed onto the substrates to fabricate electrodes with a binder and acetylene black. The incorporation of ancillary materials often results in the inadequate contact at the interfaces between electrode materials and substrate, which were inhibiting the performance of the supercapacitors. Therefore, it is urgent to explore a high-efficiency strategy for realizing in-situ construction of composite materials and using directly as high performance binder-free electrodes.

In view of the above analysis, hierarchical Ag@ $\text{Ni}(\text{OH})_2$ nanospheres have been constructed on copper substrate herein through a convenient two-step process. Galvanic replacement reaction between AgNO_3 and copper foam was exploited to generate silver nanoflowers directly on copper foam substrate. The $\text{Ni}(\text{OH})_2$ layer was constantly loaded on silver nanoflowers surface by electrodeposition. The resulting Ag@ $\text{Ni}(\text{OH})_2$ samples as binder-free electrodes exhibited enhanced electrochemical performances, which was mainly attributed to the synthesis strategy and the effective utilization of Ag as backbone. The Ag element could improve the electrical conductivity and increase the specific surface area of the active electrode material.

2. Materials and Methods

2.1. Materials

Copper substrate was carefully cleaned by toluene, acetone, ethanol and deionized water, and then immersed into HCl aqueous solution (1 M) before use in order to remove surface oxides. Silver nitrate (AgNO_3 , 99.8%), nickel nitrate ($\text{Ni}(\text{NO}_3)_2 \cdot 6\text{H}_2\text{O}$, 99%) and NaOH were used in this report.

2.2. Synthesis of Hierarchical Ag@ $\text{Ni}(\text{OH})_2$ Electrode

In a typical procedure, the precleaned copper foam was suspended and immersed into an AgNO_3 aqueous solution (0.01 M) for 10 min. After that, the copper foam with gray silver precipitates was rinsed with ethanol and deionized water, and then, a freshly prepared $\text{Ni}(\text{NO}_3)_2 \cdot 6\text{H}_2\text{O}$ aqueous solution (0.05 M) was used to deposit $\text{Ni}(\text{OH})_2$ onto the Ag core for 300 s. In the three-electrode system, the Ag/copper foam acts as working electrode, a platinum foil acts as counter electrode, and saturated calomel electrode (SCE) acts as reference electrode. The potentiostatic deposition was performed about 300 s at -1.0 V vs. SCE . At last, the resulting copper foam was rinsed with ethanol and deionized water.

2.3. Materials Characterization

The products were characterized by X-ray diffraction (XRD) using Cu $K\alpha$ radiation ($\lambda = 1.5406 \text{ \AA}$) and field-emission scanning electron microscopy (FE-SEM JEOL JSM-7610F, Japan) equipped with

an energy dispersive X-ray spectrometer (EDS). The X-ray photoelectron spectroscopy spectra (XPS) measurement was performed on an ESCALAB 250Xi (ThermoFisher Scientific Co., Ltd, USA) with Al K α as the X-ray source.

2.4. Electrochemical Measurements

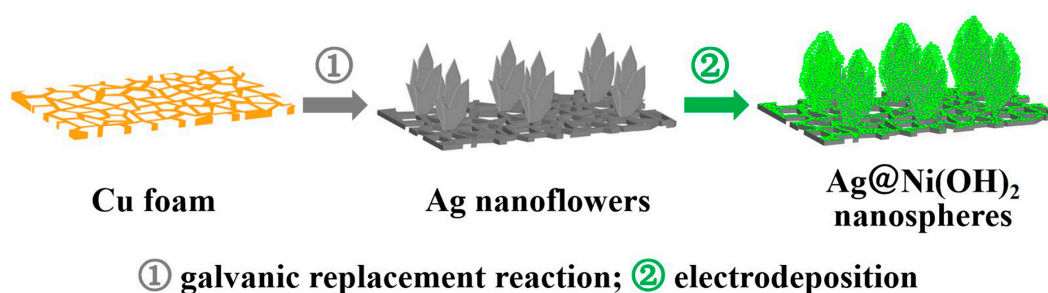
The electrochemical performance was evaluated on an electrochemical workstation (Shanghai Chenhua Instrument CHI 660D), including cyclic voltammetry (CV) and galvanostatic charge–discharge test (GCD). The three-electrode system consists of the obtained Ag@Ni(OH)₂ composite, a platinum foil and Hg/HgO (0.098 V). They serve as working electrodes, counter electrode and reference electrode, respectively. The electrolyte was a 5-M NaOH solution. The cycling performance has been assessed involving the Neware testing system.

3. Results

The construction process of Ag@Ni(OH)₂ electrode is shown in Scheme 1. Firstly, a convenient galvanic replacement reaction route is designed based on the following equation: Cu (s) + 2Ag⁺ (aq) → 2Ag (s) + Cu²⁺ (aq) [18]. Ag nanoflowers stuck to copper substrate are obtained by immersing of the copper substrate into AgNO₃ solution (0.01 M) for 10 min. In this process, copper foam acts as both reducing agent and substrate. After that, the electrochemical deposition process was performed in a three-electrode system using the Ni(NO₃)₂·6H₂O aqueous solution as electrolyte. The OH[−] generated by electrolytic reaction at the Ag electrode surface causes constant Ni(OH)₂ deposited, and thus hierarchical Ag@Ni(OH)₂ nanospheres are formed as described by the following equations [19]:



Figure 1a shows the original FE-SEM image of copper foam substrate with 3D net structure. An overview FE-SEM image of the products obtained through galvanic replacement reaction between AgNO₃ and copper foam is shown in Figure 1b, where the uniform and dense Ag nanostructure is observed on the copper substrate. The magnified image in Figure 1c shows that the products are nanoflowers, which are made up of a number of nanosheets with thickness of about 20 nm and rough surface (Figure 1d).



Scheme 1. The illustration of the in-situ construction process of core/shell structured Ag@Ni(OH)₂ electrode.

The subsequent electrochemical deposition allows the coating of uniform Ni(OH)₂ layer on the surface of Ag nanoflowers. As can be realized from Figure 2a, Ag nanoflowers are covered tightly with a dense layer of Ni(OH)₂ when the deposition time is only 30 s. The original shape of the Ag nanoflowers constructed by numbers of nanosheets is clearly visible. The corresponding EDS element mapping images and EDS spectrum (in inset of Figure 2a) confirm the existence of Cu, Ag, Ni and O elements. Further observation of the enlarged image in Figure 2b confirms that in addition to the tightly wrapped a layer of Ni(OH)₂ on the surface of the Ag nanosheets, a large number of Ni(OH)₂

nanospheres with regular shapes are deposited on the surface with a mean diameter of about 260 nm (Figure 2c).

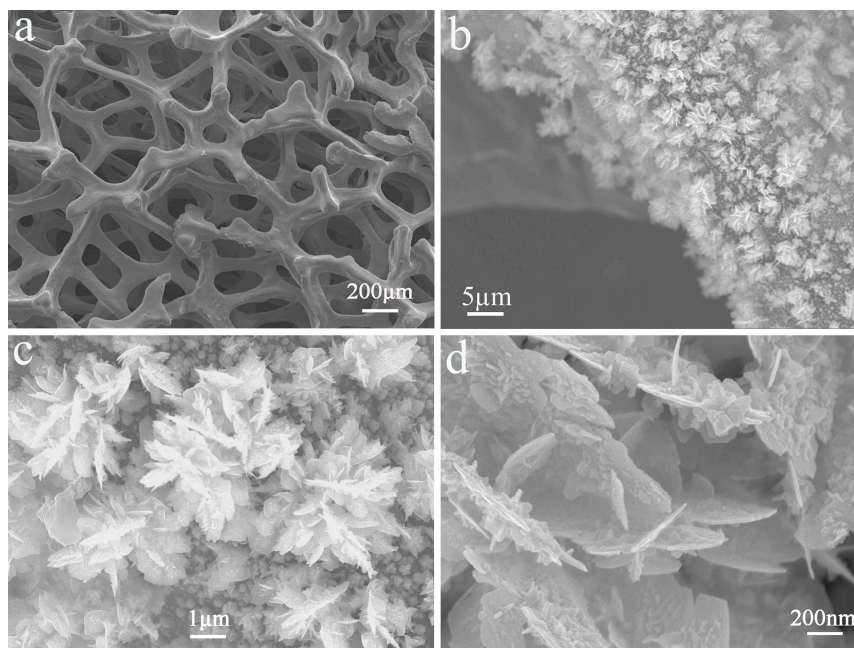


Figure 1. FE-SEM images: (a) pristine nickel foam; (b–d) Ag nanoflowers at different magnifications.

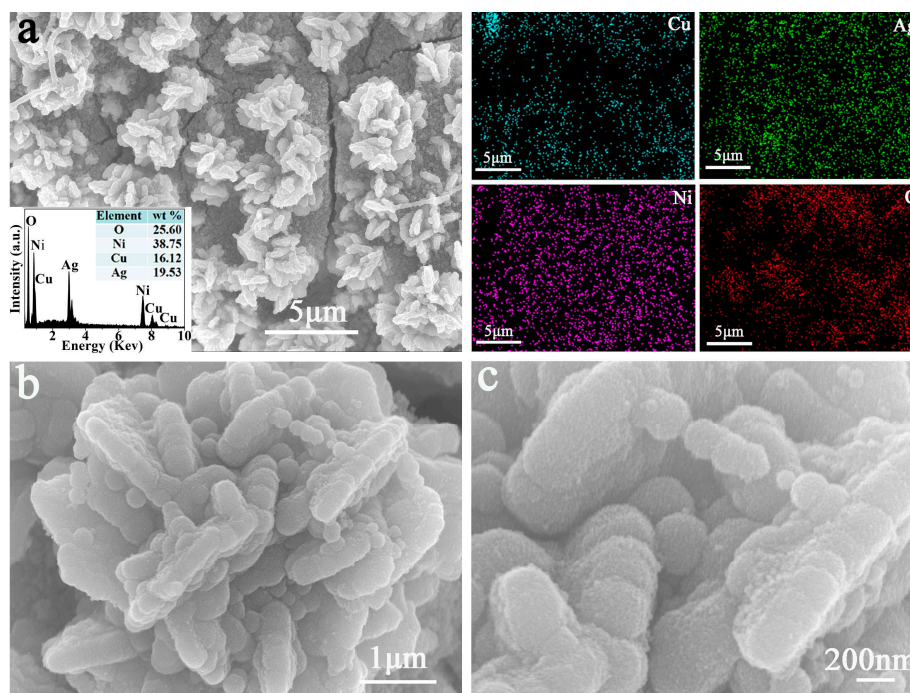


Figure 2. FE-SEM images of the Ag@Ni(OH)₂ composite with 30 s the deposition time of Ni(OH)₂: (a) Low magnification image and the EDS element mapping, inset is the EDS spectrum; (b–c) high magnification images.

When the deposition time is up to 300 s, as shown in Figure 3a, Ni(OH)₂ nanospheres with a diameter of about 650 nm are found to be packed closely with each other, and the corresponding EDS element mapping images reveal the coexistence of Cu, Ag, Ni and O elements. Figure 3b,c present the magnified images of Ni(OH)₂ nanospheres. The Ni(OH)₂ nanospheres are composed of a large

number of smaller nanoparticles with diameter of about 10 nm, which are interconnected with each other to form a worm-like structure.

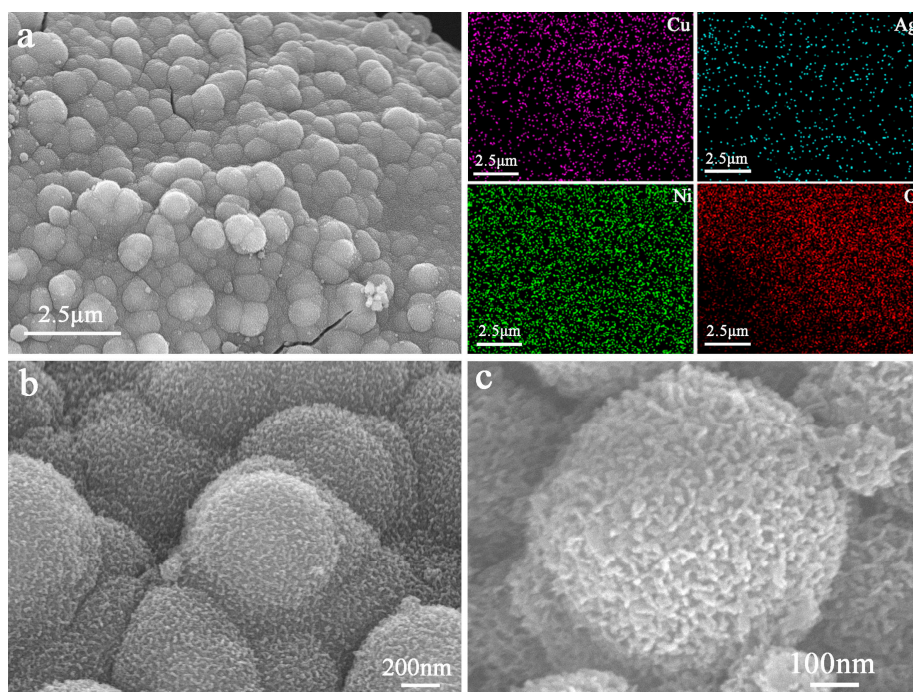


Figure 3. FE-SEM images of the Ag@Ni(OH)₂ composite with 300 s the deposition time of Ni(OH)₂: (a) Low magnification image and the EDS element mapping; (b,c) high magnification images.

Figure 4a presents the XRD patterns of Ag nanoflowers and Ag@Ni(OH)₂ composite on copper foam. Three characteristic peaks labeled with asterisks belong to the copper substrate (JCPDS card no. 01-1241), the as-synthesized Ag nanoflowers display crystalline peaks at diffraction angle of about 38.12°, 44.28° and 77.48° corresponding to (111), (200) and (311) crystalline plane, respectively, in good agreement with the face-centered cubic (fcc) Ag (JCPDS card no. 04-0783). The Ag@Ni(OH)₂ composite exhibits (100), (101) and (111) crystalline peaks at 33.52°, 38.64° and 62.66°, indicating the β phase of Ni(OH)₂ (JCPDS card no. 14-0117). XPS was carried out to further verify the deposition of Ni(OH)₂ layer on the surface of Ag nanoflowers. The survey spectrum in Figure 4b confirms the presence of C, O, Ni and Ag elements, agreeing with the EDS result. The spectrum of Ag 3d shows two peaks at 368.2 and 374.4 eV, as shown in Figure 4c, which originated from Ag 3d_{5/2} and Ag 3d_{3/2}, respectively. Figure 4d presents the Ni LMM (L-inner level-M-inner level-M-inner level electron transition) Auger spectrum with the Auger peak of 841.8 eV, the peak shape is in good agreement with the literature [20]. The spectrum of Ni 2p shows two major peaks in Figure 4e, the binding energies at 856 and 873.7 eV are ascribed to Ni 2p_{3/2} and Ni 2p_{1/2}, respectively. So the spin-orbit coupling energy separation is 17.7 eV, and the Auger parameter of Ni(OH)₂ is 1698 eV [16,20,21]. In addition, two satellite peaks at 861.7 and 880 eV correspond to the binding energies of Ni 2p_{3/2} and Ni 2p_{1/2}, respectively. The peak of O 1s spectrum located at around 531 eV can be attributed to the hydroxide (OH⁻) group [22].

The obtained hierarchical Ag@Ni(OH)₂ nanospheres sample on copper substrate was directly used as binder-free electrodes for the electrochemical performance estimation in a three-electrode system. Figure 5a displays the CV curves of different electrodes at the scan rate of 5 mV s⁻¹ at potential window of 0–0.6 V, including Ag@Ni(OH)₂ (immerse copper substrate in 0.01 M of AgNO₃ solution for 10 min and then electrodeposition of 300 s on the obtained Ag electrode surface using 0.05 M of Ni(NO₃)₂·6H₂O as electrolyte), Ni(OH)₂ (electrodeposition of 300 s on copper substrates using 0.05 M of Ni(NO₃)₂·6H₂O as electrolyte), Ag electrode (immerse copper substrate in 0.01 M of AgNO₃ solution for 10 min) and copper foam substrate. As can be seen, the CV curve integral area of the

Ag@Ni(OH)₂ electrode is much larger than those of the others, demonstrating the highest specific capacity of the Ag@Ni(OH)₂ composite electrode. The Ag@Ni(OH)₂ electrode shows two pairs of redox peaks in the voltammogram where the sharp and strong peaks at 0.5 V and 0.3 V are ascribed to the redox couple Ni²⁺/Ni³⁺, and the broad and small peaks at 0.27 V and 0.10 V are ascribed to the redox couple Ag/Ag⁺ as below [23]:

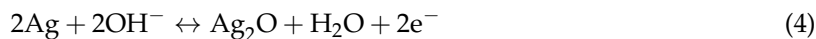


Figure 5b reveals the GCD curves of the Ag@Ni(OH)₂, Ni(OH)₂ and Ag electrode at 2 mA cm⁻², where Ag@Ni(OH)₂ electrode presents the longest discharge time, consistent with the CV measurements. It can be noticed that the intensity of redox peaks of Ag becomes weaker and weaker with the continuous deposition of Ni(OH)₂ layer (Supplementary Materials Figure S1a). The corresponding GCD curves in Figure S1b illustrate a tiny plateau at about 0.15 V, corresponding to the redox couple Ag/Ag⁺ [24–26]. As can be observed, the plateau period becomes shorter with the continuous deposition of Ni(OH)₂.

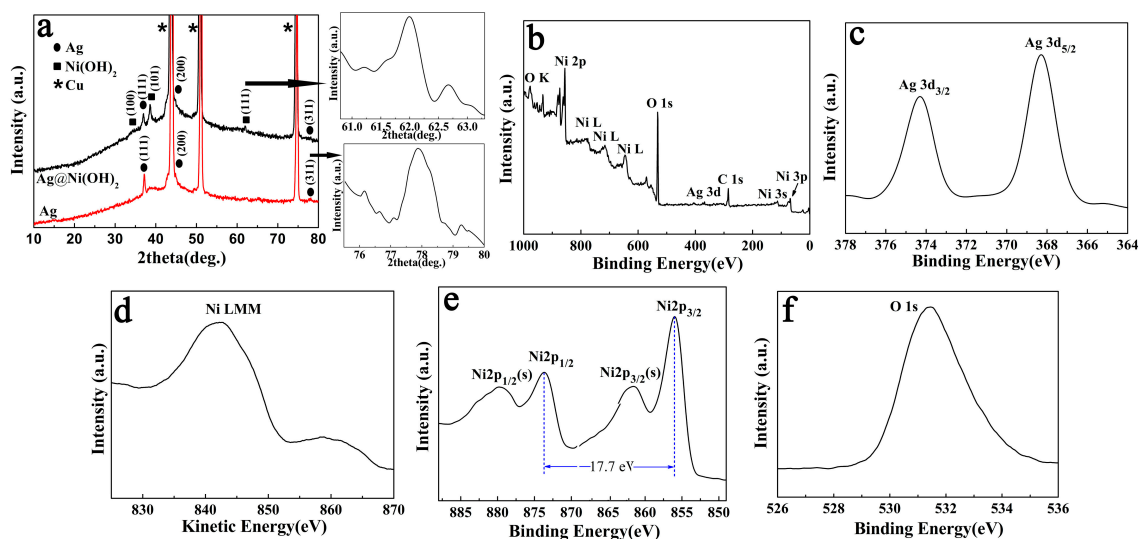


Figure 4. (a) XRD patterns of Ag and Ag@Ni(OH)₂ (The arrows point to a higher magnification); (b–f) XPS spectra of the Ag@Ni(OH)₂: survey scan, Ag 3d, Ni LMM, Ni 2p and O 1s.

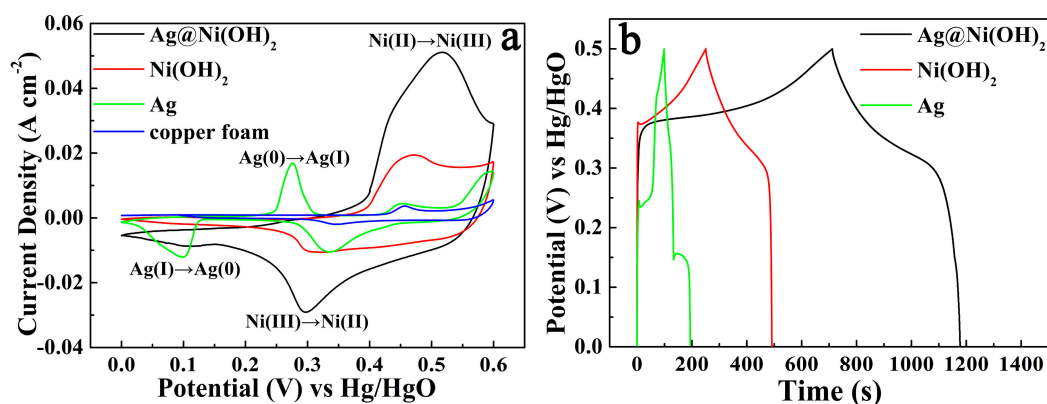


Figure 5. (a) CV curves of Ag@Ni(OH)₂, Ni(OH)₂ and Ag as electrodes, and copper foam substrate at a scan rate of 5 mV s⁻¹; (b) a comparison of GCD curves of the three electrodes.

The CV curves of the Ag@Ni(OH)₂ electrode were recorded at various scan rates ranged from 2 to 50 mV s⁻¹ within the potential range of 0–0.6 V, as seen from Figure 6a. A pair of strong redox peaks with good symmetry are observed, and all the CV curves maintain similar shape. The current response increases with scan rate, that is, the oxidation and reduction peak potentials move to more positive and negative directions, respectively, on the contrary, the specific capacitance decreases with the increase of scan rate according to the equation in Supplementary Materials. The decrease may be attributed to the fact that many internal electroactive sites of the electrode are inadequate participated in redox reactions at high scan rates due to the limitation of ionic/electronic diffusion [27]. The typical GCD tests were further performed in a potential window of 0–0.5 V at different current densities ranged from 2 to 20 mA cm⁻² (Figure 6b). The symmetric and nonlinear profile of the GCD curves exhibits good pseudo-capacitance characteristics. The specific capacitance of Ag@Ni(OH)₂ electrode can be obtained by the equation in Supplementary Materials [28]. In addition, the CV and GCD measurements of Ni(OH)₂ and Ag electrode were also performed for comparison in Figure S2. Figure 6c shows the comparative plots of the specific capacitance versus current density of Ag@Ni(OH)₂, Ni(OH)₂ and Ag electrodes. The specific capacitance values of the three electrodes are shown in Table S1 in Supplementary Materials. The specific capacitance of Ag@Ni(OH)₂ decreases from 1.864 to 0.760 F cm⁻², corresponding to the discharge current density from 2 to 20 mA cm⁻², respectively, which are much higher than Ni(OH)₂ and Ag electrodes. Meanwhile, the average equivalent series resistance (R_{ESR}) is 0.988 Ω cm⁻², the equation and data (Table S2) are displayed in Supplementary Materials [8] (Figure 6d). The low R_{ESR} is attributed to the direct growth of Ag on copper foam substrate using galvanic replacement reaction that leads to strong interaction between them. Meanwhile, the Ag nanostructures with good conductivity act as both collector and effective constituent of the active material.

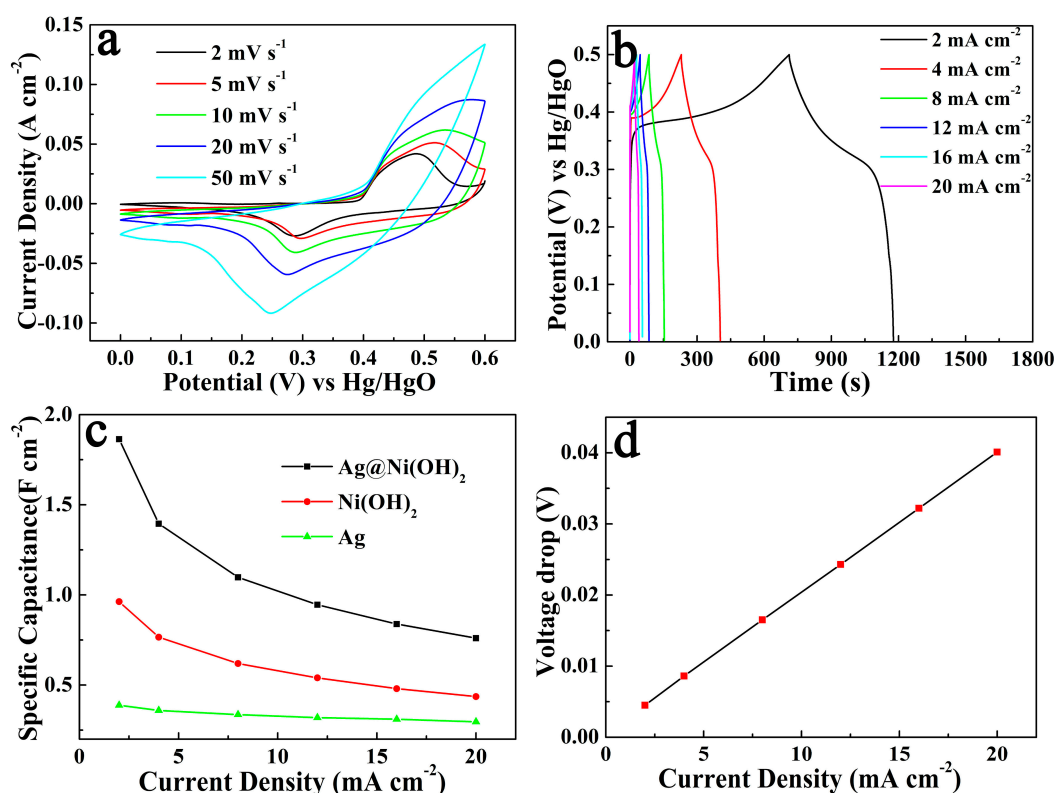


Figure 6. (a) The CV curves, (b) GCD curves, (c) plots of specific capacitance versus current density and (d) voltage drops during the GCD tests of the Ag@Ni(OH)₂ electrode.

Figure 7 shows the specific capacitance retention curve of the Ag@Ni(OH)₂ electrode. It maintains 90.43% of its original specific capacitance value and no obvious structure deformation (Figure S3) after

3000 cycles. This good cyclic property is attributed to the effective bonding between active materials and copper substrate.

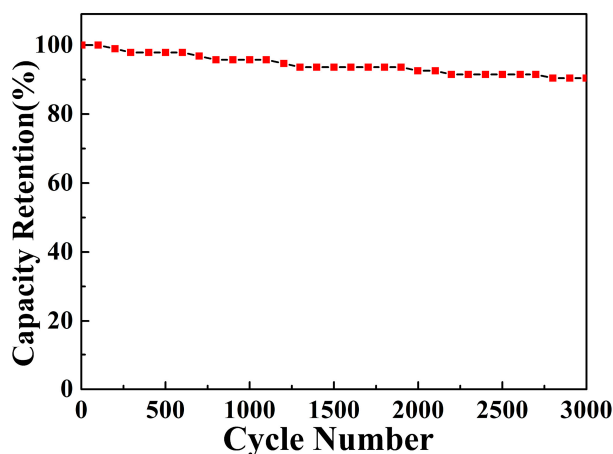


Figure 7. Cycling performances of the Ag@Ni(OH)₂ electrode.

The resulting hierarchical Ag@Ni(OH)₂ samples available in high performance binder-free electrodes may be mainly attributed to the following factors: (1) the Ag nanoflowers directly grown on copper substrate by the electroless deposition techniques reduces the contact resistance, and provides a natural pathway for electron transport thereby [22]; (2) The use of Ag nanoflowers as backbone provides adequate surface area for subsequent Ni(OH)₂ layer deposition and allows fast electric and ionic conduction through the electrode owing to its good electrical conductivity [27]; (3) The electrodeposition of Ni(OH)₂ nanospheres are composed by smaller nanoparticles, which interconnect with each other on the surface of the Ag nanoflowers and this generates abundant space, enabling the electrolyte to fully infiltrated into the internal area of the electrode, and thus ensuring full utilization of active electrode materials [29].

4. Conclusions

In summary, hierarchical Ag@Ni(OH)₂ nanospheres have been designed and in-situ constructed on copper foam substrate through the combination of electroless deposition technology with electrodeposition. Copper foam acts as both reducing agent and substrate. The resulting Ag@Ni(OH)₂ samples could be directly used as high performance binder-free electrodes and exhibited a high specific capacitance value of 1.864 F cm⁻², low R_{ESR} of 0.988 Ω cm⁻², and good cycling stability with a capacitance retention of 90.43% after 3000 cycles. The good electrochemical properties should be ascribed to the synthesis strategy and the effective utilization of Ag as backbone, which can increase the electrical conductivity and the specific surface area of the active material. Moreover, this convenient method can be extended to construct other binary or multiple composites with Ag as conductive reinforcement.

Supplementary Materials: The following are available online at <http://www.mdpi.com/2073-4352/9/2/118/s1>, Figure S1: Ag@Ni(OH)₂ electrode corresponding to different Ni(OH)₂ deposition time: (a) CV curves; (b) GCD curves. Figure S2: (a,c) The CV curves and (b,d) GCD curves of Ni(OH)₂ and the Ag electrode, respectively. Figure S3. FE-SEM images of the Ag@Ni(OH)₂ composite at different magnifications after 3000 cycles. Table S1. The specific capacitance versus current density of the three electrodes. Table S2. The R_{ESR} and voltage drop versus current density of the Ag@Ni(OH)₂ electrode. Equations for calculating specific capacitance and average equivalent series resistance.

Author Contributions: Formal analysis, Y.C.; Investigation, S.L.; Methodology, X.C. and F.Y.; Software, J.Y.; Supervision, H.W. and X.Y.; Writing—original draft, S.L.; Writing—review&editing, X.Y.

Funding: This research was funded by The National Key Technology R&D Program of China (Grant No. 2016YFB0401103) and National Natural Science Foundation of China (Grant No. 51672103).

Conflicts of Interest: The authors declare no conflicts of interest.

References

1. Saha, S.; Samanta, P.; Murmu, N.C.; Kuila, T. A review on the heterostructure nanomaterials for supercapacitor application. *J. Energy Storage* **2018**, *17*, 181–202. [[CrossRef](#)]
2. Guo, J.X.; Zhang, X.Q.; Sun, Y.F.; Zhang, X.H.; Tang, L.; Zhang, X. Double-shell CuS nanocages as advanced supercapacitor electrode materials. *J. Power Sources* **2017**, *355*, 31–35. [[CrossRef](#)]
3. Dai, X.; Chen, D.; Fan, H.Q.; Zhong, Y.; Chang, L.; Shao, H.B.; Wang, J.M.; Zhang, J.Q.; Cao, C.N. Ni(OH)₂/NiO/Ni composite nanotube arrays for high-performance supercapacitors. *Electrochim. Acta* **2015**, *154*, 128–135. [[CrossRef](#)]
4. Liu, G.L.; Zhao, C.; Liu, T.Y.; He, D.; Suo, H. Facile route to achieve book-like tricobalt tetraoxide microstructures on copper foam for high performance supercapacitor. *Mater. Lett.* **2018**, *220*, 78–81. [[CrossRef](#)]
5. Gao, L.; Zhang, L.L.; Jia, S.Y.; Liu, X.C.; Wang, Y.H.; Xing, S.X. Facile route to achieve hierarchical hollow MnO₂ nanostructures. *Electrochim. Acta* **2016**, *203*, 59–65. [[CrossRef](#)]
6. Wang, T.; Pan, J.Q.; Achille, G.K.; Sun, Y.Z. A green dual complexation precipitation synthesis of hierarchical α -Ni(OH)₂ microspheres and their electrochemical performance. *Int. J. Hydrogen Energy* **2017**, *42*, 19139–19147. [[CrossRef](#)]
7. Wiston, B.R.; Ashok, M. Electrochemical performance of nickel hydroxide nanopetals for supercapacitor electrodes. *Mater. Lett.* **2019**, *235*, 76–79. [[CrossRef](#)]
8. He, D.; Wang, G.D.; Liu, G.L.; Suo, H.; Zhao, C. Construction of leaf-like CuO-Cu₂O nanocomposite on copper foam for high-performance supercapacitors. *Dalton Trans.* **2017**, *46*, 3318–3324. [[CrossRef](#)] [[PubMed](#)]
9. Khatavkar, S.N.; Sartale, S.D. α -Fe₂O₃ thin film on stainless steel mesh: A flexible electrode for supercapacitor. *Mater. Chem. Phys.* **2019**, *225*, 284–291. [[CrossRef](#)]
10. Lu, H.C.; Chen, J.Z.; Tian, Q.H. Wearable high-performance supercapacitors based on Ni-coated cotton textile with low-crystalline Ni-Al layered double hydroxide nanoparticles. *J. Colloid Interface Sci.* **2018**, *513*, 342–348. [[CrossRef](#)] [[PubMed](#)]
11. Yao, L.Q.; Cheng, T.; Shen, X.Q.; Zhang, Y.Z.; Lai, W.Y.; Huang, W. Paper-based all-solid-state flexible asymmetric micro-supercapacitors fabricated by a simple pencil drawing methodology. *Chin. Chem. Lett.* **2018**, *29*, 587–591. [[CrossRef](#)]
12. Shi, D.; Zhang, L.; Yin, X.; Huang, T.; Gong, H. One step processed advanced interwoven architecture of Ni(OH)₂ and Cu nanosheets with ultrahigh supercapacitor performance. *J. Mater. Chem. A* **2016**, *4*, 12144–12151. [[CrossRef](#)]
13. Jeyasubramanian, K.; Gokul Raja, T.S.; Purushothaman, S.; Kumar, M.V.; Sushmitha, I. Supercapacitive performances of MnO₂ nanostructures grown on hierarchical Cu nano leaves via electrodeposition. *Electrochim. Acta* **2017**, *227*, 401–409. [[CrossRef](#)]
14. Pawar, S.A.; Patil, D.S.; Shin, J.C. Hexagonal sheets of Co₃O₄ and Co₃O₄-Ag for high-performance electrochemical supercapacitors. *J. Ind. Eng. Chem.* **2017**, *54*, 162–173. [[CrossRef](#)]
15. Zhang, L.Y.; Shi, D.W.; Huang, T.J.; Huang, R.Z.; Gong, H. Light enhanced energy storage ability through hybrid plasmonic Ag nanowires decorated hydroxide “skin structure”. *Nanoscale* **2017**, *9*, 18430–18437. [[CrossRef](#)] [[PubMed](#)]
16. Yuksel, R.; Coskun, S.; Kalay, Y.E.; Unalan, H.E. Flexible, silver nanowire network nickel hydroxide core-shell electrodes for supercapacitors. *J. Power Sources* **2016**, *328*, 167–173. [[CrossRef](#)]
17. Du, H.J.; Pan, Y.; Zhang, X.; Cao, F.Y.; Wan, T.; Du, H.W.; Joshi, R.; Chu, D.W. Silver nanowire/nickel hydroxide nanosheet composite for a transparent electrode and all-solid-state supercapacitor. *Nanoscale Adv.* **2019**, *1*, 140–146. [[CrossRef](#)]
18. Wu, G.X.; Yang, S.J.; Liu, Q.M. Synthesis of silver nanostructures by simple redox under electrodeposited copper microcubes and the orient attachment growth of 2D silver. *Appl. Surf. Sci.* **2015**, *357*, 583–592. [[CrossRef](#)]
19. Lo, I.H.; Wang, J.Y.; Huang, K.Y.; Huang, J.H.; Kang, W.P. Synthesis of Ni(OH)₂ nanoflakes on ZnO nanowires by pulse electrodeposition for high-performance supercapacitors. *J. Power Sources* **2016**, *308*, 29–36. [[CrossRef](#)]

20. Biesinger, M.C.; Lau, L.M.; Gerson, A.R.; Smart, R.C. The role of the Auger parameter in XPS studies of nickel metal, halides and oxides. *Phys. Chem. Chem. Phys.* **2012**, *14*, 2434–2442. [[CrossRef](#)] [[PubMed](#)]
21. Gou, J.X.; Xie, S.L.; Liu, C.G. Flower-like Ni–Co hydroxides on Ni foam for high-performance supercapacitor applications. *New J. Chem.* **2018**, *42*, 4175–4181. [[CrossRef](#)]
22. Sekhar, S.C.; Nagaraju, G.; Yu, J.S. Conductive silver nanowires-fenced carbon cloth fibers-supported layered double hydroxide nanosheets as a flexible and binder-free electrode for high-performance asymmetric supercapacitors. *Nano Energy* **2017**, *36*, 58–67. [[CrossRef](#)]
23. Park, S.; Ming Tan, A.W.; Wang, J.X.; Lee, P.S. Coaxial Ag-base metal nanowire networks with high electrochemical stability for transparent and stretchable asymmetric supercapacitors. *Nanoscale Horiz.* **2017**, *2*, 199–204. [[CrossRef](#)]
24. Cao, F.H.; Wang, Z.H.; Wang, Y.Z.; Yan, Y.M.; Liu, M.T.; Li, L.; Ao, G.H.; Chen, K.F.; Lv, Z. In situ fabrication of cellular architecture on silver metals using methane/oxygen gas mixture and its application for energy storage. *Electrochim. Acta* **2018**, *280*, 25–32. [[CrossRef](#)]
25. Liu, P.P.; Liu, J.; Cheng, S.; Cai, W.Z.; Yu, F.Y.; Zhang, Y.P.; Wu, P.; Liu, M.L. A high-performance electrode for supercapacitors: Silver nanoparticles grown on a porous perovskite-type material $\text{La}_{0.7}\text{Sr}_{0.3}\text{CoO}_{3-\delta}$ substrate. *Chem. Eng. J.* **2017**, *328*, 1–10. [[CrossRef](#)]
26. Usman, M.; Pan, L.J.; Sohail, A.; Mahmood, Z.; Cui, R.X. Fabrication of 3D vertically aligned silver nanoplates on nickel foam-graphene substrate by a novel electrodeposition with sonication for efficient supercapacitors. *Chem. Eng. J.* **2017**, *311*, 359–366. [[CrossRef](#)]
27. Shakir, I.; Ali, Z.; Bae, J.; Park, J.; Kang, D.J. Conformal coating of ultrathin $\text{Ni}(\text{OH})_2$ on ZnO nanowires grown on textile fiber for efficient flexible energy storage devices. *RSC Adv.* **2014**, *4*, 6324–6329. [[CrossRef](#)]
28. Jia, X.-X.; Wu, X.; Liu, B.-D. Formation of $\text{ZnCo}_2\text{O}_4@ \text{MnO}_2$ core-shell electrode materials for hybrid supercapacitor. *Dalton Trans.* **2018**, *47*, 15506–15511. [[CrossRef](#)] [[PubMed](#)]
29. Xing, Z.C.; Chu, Q.X.; Ren, X.B.; Ge, C.J.; Qusti, A.H.; Asiri, A.M.; Al-Youb, A.O.; Sun, X.P. Ni_3S_2 coated ZnO array for high-performance supercapacitors. *J. Power Sources* **2014**, *245*, 463–467. [[CrossRef](#)]



© 2019 by the authors. Licensee MDPI, Basel, Switzerland. This article is an open access article distributed under the terms and conditions of the Creative Commons Attribution (CC BY) license (<http://creativecommons.org/licenses/by/4.0/>).